# Entropic and Energetic Selectivity in Air Separation with Microporous Materials

**Premkumar S. Rallabandi and David M. Ford**
Dept. of Chemical Engineering, Texas A&M University, College Station, TX 77843

*Materials such as zeolites, carbon molecular sieves, and polymers are used increasingly in the separation of air, based on the difference in diffusion rate between oxygen and nitrogen through the material. The design of improved materials requires knowledge of the molecular-level phenomena responsible for the separation, particularly relative roles of energetic and entropic (confinement) effects. This issue is difficult to resolve experimentally, as evidenced by the wide range in reported literature values reviewed here. A complementary approach is taken based on a combination of molecular modeling, statistical mechanics, and transition-state theory. Selectivities for molecular models of oxygen and nitrogen in microporous structures are calculated using a Monte Carlo technique and resolved into entropic and energetic components, for a range of pore window sizes. Atomic-level flexibility (vibration) is considered as well. The calculated entropic selectivities are significantly lower than reported theoretical results, but still consistent with experimental data. The energetic selectivity is very sensitive to the window dimensions and flexibility, but the entropic contribution is much less affected. This also contradicts some previous assumptions in the literature.*

## Introduction

The separation of gas mixtures based on differences in the diffusion rates of the constituent species through a microporous medium is a topic of great technological and scientific importance (Karger and Ruthven, 1992). An effective diffusivity-based separation requires a medium with pores small enough to discriminate among the different components. Separations become very challenging when the sizes of the species in the mixture are very similar, as in the case of oxygen and nitrogen. Certain zeolites and carbon molecular sieves (CMS) have pore sizes comparable to the dimensions of those molecules and, hence, are employed in the separation of air, typically in a pressure swing adsorption process (Gaffney, 1996). In the last two decades, glassy polymers in membrane form have also become quite attractive as gas separation media. Owing to certain advantages, such as ease of operation and low capital requirements, polymeric membrane-based technology is increasingly employed in industrial applications (Stern, 1994).

A trade-off between permeability and selectivity is a limitation often encountered in the design of materials for kinetic (diffusion-based) separations; in order to increase the selectivity, the magnitude of the diffusion barrier must be increased (that is, the ''pore size'' must be reduced). Robeson (1991) demonstrated this permeability-selectivity tradeoff in kinetic separations on polymeric materials. Singh and Koros (1996) pointed out that the upper bound on the performance of polymeric membranes falls short of the economically attractive region presently occupied by inorganic materials. Furthermore, these authors analyzed experimental data within the framework of transition state theory to obtain the individual energetic and entropic contribution to selectivity in the oxygen/nitrogen separation. From their regression calculations for zeolite 4A, CMS and the glassy polymer polypyrrolone, Singh and Koros observed that the energetic selectivities in the inorganic sieves and polymers were of comparable magnitude, but that the performance of the inorganic materials was far superior in terms of entropic selectivity. The authors surmised that this result was due to inherent differences in the molecular-level rigidity of the host materials; the inorganic materials could effectively limit the rotation of the nitrogen molecule in the transition state, while the polymer could not, due to the larger thermal fluctuations in the polymer matrix.

Correspondence concerning this article should be addressed to D. M. Ford.

The findings of Singh and Koros (1996) are intriguing. However, as will be shown in the next section, scatter in the experimental data in the literature makes it difficult to reach any specific conclusions which would impact materials design. We believe that approaches which employ molecular modeling and statistical mechanics will be instrumental to further progress in this area. In this article, we apply these tools to obtain a fundamental understanding of the energetic and entropic contributions in the separation of oxygen and nitrogen. One of the important contributions of this work is the consideration of the effects of matrix flexibility. Even for crystalline inorganic solids, the concept of a thermally activated ''breathing motion'' of zeolite pores has been used in the literature to explain the discrepancy in window sizes measured using crystallography and permeation experiments. A simulation study based on crystal dynamics by Deem et al. (1992) indeed revealed periodic fluctuations of aperture dimensions in a variety of zeolite structures. We consider a wide range of flexibility in our model systems.

A survey of experimental results from the literature for oxygen/nitrogen separations in zeolite 4A and CMS is presented, and their implications on our current theoretical understanding are discussed. Expressions are developed for the oxygen/nitrogen selectivity of a microporous material from classical ''first principles,'' based on the transition state theory and full statistical mechanical partition functions. We also discuss how these expressions are related to some commonly used absolute rate theory formulas in the literature. Details are given for the particular molecular-level models and simulation methods employed here.

## Survey of Literature Data

Several research groups have measured the diffusion coefficients of oxygen and nitrogen in zeolite 4A and CMS materials (Ruthven and Derrah, 1975; Chihara et al., 1978; Chihara and Suzuki, 1979; Haq and Ruthven, 1986; Ruthven, 1986; Chagger et al., 1995; Farooq, 1995; Reid et al., 1998). These measurements are commonly performed using volumetric, gravimetric, flow calorimetric, or chromatographic techniques. The chromatographic method is simpler, quicker, and gives more accurate results than conventional uptake measurement techniques (Haq and Ruthven, 1986). This method is especially useful for measurements involving smaller species which adsorb weakly and diffuse at high rates. Gravimetric and volumetric methods have complementary advantages and disadvantages, but the former is more suitable for oxygen and nitrogen diffusion measurements (Chagger et al., 1995). Although flow calorimetry has also been employed in diffusion measurements of these species in CMS, accurate analysis requires the use of several complex heat- and mass-transfer corrections to the data (Chagger et al., 1995).

The diffusion coefficients are usually interpreted in the context of an activated process, where the diffusivity for species $i$ can be expressed as

$$D_i = D_{0,i} \exp\left(-U_{a,i}/k_B T\right) \tag{1}$$

where $D_{0,i}$ is frequency factor, $U_{a,i}$ is the activation energy, $k_B$ is the Boltzmann constant, and $T$ is the temperature. Following Glasstone et al. (1941), transition state theory (TST) may be used to express the frequency factor in terms of an entropic barrier $S_{a,i}$

$$D_{0,i} = e\delta_i^2 \frac{k_B T}{h} \exp\left(S_{a,i}/k_B\right) \tag{2}$$

where $\delta_i$ is the jump length and $h$ is the Planck constant. The entropic term can be thought of as quantifying the difference in the degree of confinement of the molecule between the transition state and the minimum. In many cases (such as oxygen and nitrogen), the jump lengths $\delta_i$ will be equal to a good approximation. The diffusivity selectivity for two species $A$ and $B$ can then be expressed as

$$\frac{D_A}{D_B} = \exp\left[\left(S_{a,A} - S_{a,B}\right)/k_B\right] \exp\left[-\left(U_{a,A} - U_{a,B}\right)/k_B T\right] \tag{3}$$

By measuring the diffusivities of both gases at several temperatures, one can calculate both the entropic and energetic contributions to selectivity through a regression analysis. Such data from various sources in the literature are summarized in Tables 1a and 1b, for zeolite 4A and CMS, respectively. For the sake of consistency, only those data where both oxygen and nitrogen diffusivities are measured in the same study on the same sample(s) are included in these tables. From the tables, it is clear that energetic selectivity generally favors oxygen. However, the same cannot be said for entropic selectivity. Interestingly, two of the studies on zeolite 4A show that the entropic selectivity for oxygen is less than unity (that is, nitrogen is entropically favored). The results are mixed for CMS, but most reported values of entropic selectivity are greater than one. The most striking feature of these data is the wide range of results obtained for the two components of selectivity for systems which are ostensibly quite similar. The two extreme cases are the studies of Farooq and Chagger et al., in which extremely high energetic and entropic selectivities, respectively, are reported; in each case, the high value is counterbalanced by a corresponding low value for the other factor, suggesting that the two factors are highly correlated. Also striking is how often values of entropic selectivity significantly smaller than one are reported; such results are some-

**Table 1a. Entropic and Energetic Contributions to Oxygen/Nitrogen Selectivity (Eq. 3) Measured in Zeolite 4A Near 300 K**

| Investigators | Method | Entropic Selectivity | Energetic Selectivity | Temp. $N_2$ | Range $O_2$ |
|---|---|---|---|---|---|
| Ruthven and Derrah (1975) | Grav. | 6.875 | 13.923 | 205–247 | 217–278 |
| Haq and Ruthven (1986) | Chrom. | 0.163 | 27.234 | 303–364 | 298–363 |
| Farooq* (1995) | Chrom. | 0.023 | 3,191.68 | 303–333 | 318–343 |

*Values measured in RS-10, a modified form of zeolite 4A.

**Table 1b. Entropic and Energetic Contributions to Oxygen/Nitrogen Selectivity (Eq. 3) Measured in CMS near 300 K**

| Investigators | Method | Entropic Selectivity | Energetic Selectivity | Temp. $N_2$ | Range $O_2$ |
|---|---|---|---|---|---|
| Chihara et al. (1978) | chrom. | 0.253 | 12.380 | 294–321 | 291–323 |
| Chihara and Suzuki (1979) | chrom. | | | | |
| Regenerated | | 0.607 | 7.785 | 298–358 | 297–358 |
| Treated | | 1.115 | 3.826 | 299–351 | 299–380 |
| Ruthven (1986) | grav. | 6.229 | 4.950 | 273–333 | 273–333 |
| Chagger et al. (1995) | grav. | | | | |
| Coconut derived | ads. | 5.384 | 2.091 | 275–333 | 275–333 |
| | des. | 462.500 | 0.253 | 275–333 | 275–333 |
| Coal derived | ads. | 6.875 | 1.461 | 275–333 | 275–333 |
| Reid et al.* (1998) | grav. | 0.931 | 5.723 | 273–313 | 303–343 |

*Values given are from adsorption kinetics ($k = k_0 e^{-\beta U_a}$) and not diffusion coefficient measurements. Hence, the values in the third column are the ratios of the corresponding pre-exponential factors.

what difficult to justify on a physical basis, considering that an oxygen molecule is ''smaller'' than a nitrogen molecule. Overall, these results suggest that a clear distinction between entropic and energetic effects in this separation is difficult to resolve from experiment. These experiments are challenging, and interpretation of the data may rely on assumptions about adsorption isotherms, diffusion models, and heat-transfer effects, as well as curve fitting and extrapolation. We believe that molecular modeling can contribute greatly to the understanding of energetic and entropic phenomena in diffusion-based separations, and thus can significantly impact materials design.

## Theory

### *Diffusivity selectivity from transition state theory and statistical mechanics*

In this section, we use the principles of transition state theory (TST) and statistical mechanics to derive a rigorous expression for the calculation of selectivity. The derivation is restricted to diatomic molecules modeled as rigid dumbbells, which should be appropriate for oxygen and nitrogen. The microporous solid is considered to be an isotropic network of three-dimensional adsorption sites or ''cages'' connected by narrow 2-D ''windows'' through which the penetrant passes in the course of diffusion. For notational convenience only, we consider an adsorption site to have dimensions $L \times L \times L = V$ and a window to have dimensions $W \times W = A$. The details of these cages and windows are not important at this time; a specific model will be employed later. The gases are assumed to be infinitely dilute in the solid; no interactions among gas molecules are considered.

In the TST formalism, the rate of transfer of a molecule from one adsorption site to another through a window is given by

$$k^{TST} = \frac{k_B T}{h} \frac{Q_A}{Q_V} \tag{4}$$

where $Q_A$ is the statistical mechanical partition function for a molecule confined to the window, and $Q_V$ is the partition function for a molecule in the adsorption site (Hill, 1986; Snurr et al., 1994). The rate constant(s) can generally be related to a diffusion coefficient; if the pore structure is geometrically regular, the relationship may be very simple. For example, if we have a set of identical adsorption sites arranged on a cubic lattice, the diffusion coefficient is given by

$$D = \frac{\delta^2}{6} k^{TST} \tag{5}$$

where $\delta$ is the length scale associated with the jump (Auerbach and Metiu, 1996). In the context of our model, $\delta$ can be taken as the center-to-center distance of the adjacent cages. Now, we explicitly consider a rigid diatomic molecule moving between two neighboring cages. The full expressions for $Q_A$ and $Q_V$ are given in Appendix A. Based on Eqs. 4, A3–A5, and A7–A9, we may write

$$k^{TST} = (2\pi\beta m)^{-1/2} \frac{Z_A}{Z_V} \tag{6}$$

where $m$ is the mass of the molecule, $Z_A$ is the configurational partition function for a molecule confined to the window, and $Z_V$ is the configurational partition function for a molecule in the adsorption site. These configurational partition functions completely account for the molecular-level energetic interactions between the gas molecule and the solid (see Appendix A for full definitions). Assuming $\delta$ to be the same for both oxygen and nitrogen, Eqs. 5 and 6 can be used to write an expression for the diffusivity selectivity

$$\frac{D_{O_2}}{D_{N_2}} = \frac{k^{TST}_{O_2}}{k^{TST}_{N_2}} = \left(\frac{m_{O_2}}{m_{N_2}}\right)^{-1/2} \frac{Z_{A,O_2} Z_{V,N_2}}{Z_{A,N_2} Z_{V,O_2}} \tag{7}$$

Any of the configurational partition functions can be related to a corresponding excess Helmholtz free energy (McQuarrie, 1976), as $Z = \exp(-\beta A^{ex})$, with $\beta = 1/k_B T$. This free energy is ''excess'' in the sense that it arises from the interaction of the gas molecule with the solid; thus, the reference state is an ideal gas with no solid present. Equation 7 can therefore also be written

$$\frac{D_{O_2}}{D_{N_2}} = \left(\frac{m_{O_2}}{m_{N_2}}\right)^{-1/2} \exp\left[-\beta\left(A^{ex}_{O_2} - A^{ex}_{N_2}\right)\big|_A\right] \times \exp\left[\beta\left(A^{ex}_{O_2} - A^{ex}_{N_2}\right)\big|_V\right] \tag{8}$$

where the subscripts $A$ and $V$ represent evaluation in the window and in the adsorption site, respectively. Recognizing that Eq. 8 can be rewritten in terms of free energies of activation, and that the mass ratio prefactor is simply the ideal contribution, one may obtain Eq. 3 using the fundamental thermodynamic relation $A = U - TS$.

At this point, however, we make the further assumption that the difference between the free energies of oxygen and nitrogen in the adsorption site is small compared to the difference in the window. This is done for the sake of physical simplicity only; the more general case can easily be studied as well. The quality of this assumption, of course, depends strongly on the structure of the solid adsorbent. The assumption is likely to be a good one for zeolite 4A, where the cages are relatively large ($L \approx 13$ Å) and the windows are small. The assumption is probably not unreasonable for CMS as well. The applicability to polymers, where the cavities can be quite small, is more questionable. In any case, with this assumption, Eqs. 7 and 8 reduce to

$$\frac{D_{O_2}}{D_{N_2}} \approx \left(\frac{m_{O_2}}{m_{N_2}}\right)^{-1/2} \exp\left[-\beta\left(A^{ex}_{O_2} - A^{ex}_{N_2}\right)|_A\right] = \left(\frac{m_{O_2}}{m_{N_2}}\right)^{-1/2} \frac{Z_{A,O_2}}{Z_{A,N_2}} \quad (9)$$

Equation 9, which relates the selectivity to the excess free energy difference between oxygen and nitrogen in the window, will be the basis for our calculations with a molecular-level model of a pore constriction. The mass ratio prefactor can be recognized as the Knudsen contribution to selectivity (Karger and Ruthven, 1992); when there is little difference in excess free energy between oxygen and nitrogen in the windows of the microporous solid, this will be the dominant separation mechanism. Since its value (0.935) is close to unity, it is largely neglected in the following discussion.

### *Previous absolute rate theory approaches*

We have written in full molecular-level detail the partition functions which must be evaluated to estimate the diffusion selectivity (see Appendix A). Another popular approach (Ruthven and Derrah, 1972; Singh and Koros, 1996) is to make assumptions about the nature of the adsorption sites or windows that lead directly to simpler forms for the partition functions. For example, the total partition functions in the cage and the window might be written as

$$Q_V = \left[\left(\frac{2\pi m k_B T}{h^2}\right)^{1/2} L\right]^3 \left[\left(\frac{8\pi^2 I k_B T}{h^2}\right)^{1/2}\right]^2 \exp\left(-\beta \overline{U}_V\right) \quad (10)$$

$$Q_A = [q_{\text{trans/vib}}]^2 [q_{\text{rot/vib}}]^2 \exp\left(-\beta \overline{U}_A\right) \quad (11)$$

where $\overline{U}_V$ and $\overline{U}_A$ are the average potential energies of the gas molecule in the cage and the window, respectively. Equation 10 may be obtained directly from Eqs. A3–A5, with the assumption that the potential energy of the molecule throughout the adsorption site is well-represented by some average value $\overline{U}_V$, irrespective of its position and orientation. This is probably a reasonable assumption for fairly large adsorption sites or cages. This description of a molecule confined to the window requires more detail and insight, since translation and rotation may be significantly hindered for some molecules. Indeed, these modes of motion may become vibrational in nature within the window; this fact is reflected in the more general rotation used in Eq. 11. Because of their simple form, equations like Eqs. 10 and 11 have served as the starting point for further analysis and simplification. A wide range of assumptions have been made regarding the translational and rotational contributions within the window. For example, the translational degrees of freedom have been ignored (Singh and Koros, 1996), and they have been replaced by vibrations (Ruthven and Derrah, 1972). Rotational motion has been considered free (Ruthven and Derrah, 1972; Singh and Koros, 1996), replaced by vibration (Singh and Koros, 1996), and ignored (Singh and Koros, 1996) in different situations. We discuss below one such treatment in the literature, which is particularly relevant to the present study because it addresses the oxygen/nitrogen separation.

Singh and Koros (1996) have considered the mechanism of air separation in zeolite A in the context of TST and equations similar to Eqs. 10 and 11. In particular, they estimated the selectivity for a situation where oxygen is freely rotating within a window, but the rotation of nitrogen is so hindered as to become vibrational. Thus, the partition function $q_{\text{rot/vib}}$ for oxygen was taken to be the same as that given in Eq. 10 for free rotation, but $q_{\text{rot/vib}}$ for nitrogen was estimated using a vibrational partition function (McQuarrie, 1976). In order to evaluate this partition function, the vibrational frequencies of nitrogen along the corresponding degrees of freedom were approximated using equilibrium sorption data for nitrogen in mordenite; direct experimental information about the frequencies in the zeolite A windows is perhaps impossible to obtain, since these transition states are so short-lived. Furthermore, Singh and Koros assumed that $q_{\text{trans/vib}}$ for both oxygen and nitrogen in the window could simply be neglected. This is perhaps not a good assumption, since the postulation of free rotation for oxygen would seem to imply some significant translational freedom within the window as well. With these assumptions, Singh and Koros found a value of 14.6 for the entropic selectivity in the oxygen/nitrogen separation. The inclusion of the effects of $q_{\text{trans/vib}}$ would likely increase this estimate.

## Model and Simulation Details

### *Model systems*

*Pore Structure.* We have evaluated separation selectivities in a model window which is representative of a zeolite structure. The window is an 8-member ring, with the centers of the spheres on the corners of an octagon in the $xy$ plane (Figure 1). The measure of size $W$ of this pore is illustrated in the figure. For simplicity, no ''pore body'' was explicitly constructed; only the isolated window was considered. For this model, the window surface is the octagon with the centers of the atoms at its corners.

To study the effects of flexibility in the solid matrix, we have considered mobile window atoms in the model. The

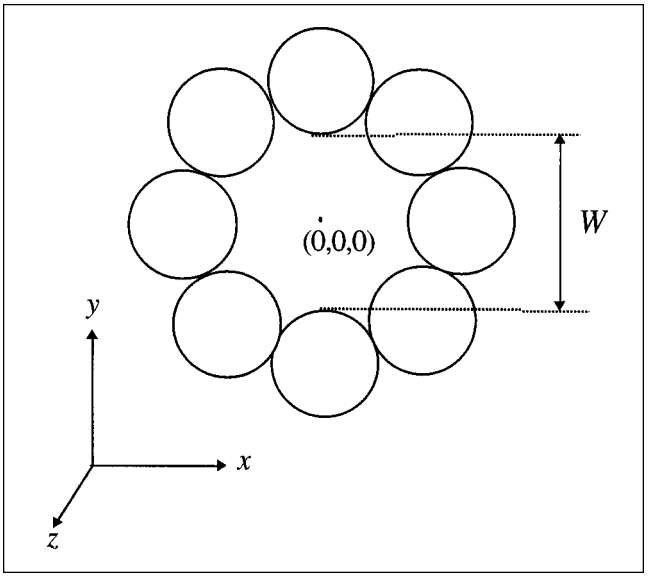


**Figure 1. Pore window modeled as an 8-member ring comprised of methyl units.**

The window opening has size $W$, as taken between the "edges" of the two opposing window atoms. The diameter of a methyl unit as shown in the figure is equal to its Lennard-Jones diameter.

atoms that make up the window were tethered to their equilibrium positions; motion of the window atoms was allowed in all three dimensions. A simple spring potential

$$U_{\text{bond}} = kd^2 \tag{12}$$

was used to tether a window atom to its anchor point: $k$ is the spring constant; $d$ is the distance between the center of the window atom and its equilibrium position. In addition to the completely rigid pore (reported as $k = \infty$), we modeled windows with $k = 66.3$, 20.0, and 6.63 (kcal mol$^{-1}$ Å$^{-2}$). The first value is about 1/20th of the typical carbon-carbon bond strength (Boyd and Pant, 1991), while the last value represents a highly flexible motion, perhaps a loose torsional mode in a polymer.

*Potentials.* The oxygen and nitrogen penetrants were modeled as rigid dumbbells with fixed lengths, and the wall atoms were modeled as united methyl units. The 12-6 Lennard-Jones (LJ) potential with a cutoff was used to model the energetic interactions between the atoms of the penetrants and the atoms of the solid. To avoid the occurrence of discontinuity in the energy at the potential cutoff, the attractive tail of the potential was modeled as a quintic spline (Theodorou and Suter, 1986). The detailed form of the potential is given in Appendix B. We note here that simulations with the full, infinite-range LJ potential yielded results that were almost identical to those obtained using the modified potential. The pure component LJ parameters for the different species are given in Table 2. The pure component parameters for oxygen and nitrogen were taken from the AMBER force field (Weiner et al., 1986), and those for the methyl units were taken from Boyd and Pant (1991). The cross interaction parameters were calculated using the usual Lorentz-Berthelot combining rules (Allen and Tildesley, 1987).

In addition to the solid model comprised of methyl units, we considered the same model comprised of oxygen atoms. The parameters used for the solid oxygen atoms were the same as those for atomic oxygen given in Table 2. The pore size was defined in the same way as pictured in Figure 1, based on the distances between "edges" of opposing oxygen atoms. The results were qualitatively very similar, so only the results for the methyl units are presented in this article; we briefly discuss the quantitative differences here. The entropic selectivities were seen to be slightly higher for the oxygen model, but differences were less than 10% across the range of pore sizes studied. This is not very surprising because, as will be discussed later, entropic selectivity is not very sensitive to the potential parameters. On the other other hand, energetic selectivities were in some cases significantly different in windows comprised of oxygen atoms; the value was higher by as much as 100% for a 3.0 Å pore and lower by about 10% for a 4.2 Å pore.

Although the AMBER force-fields are generally quite accurate, these interaction parameters and potentials have not been optimized to match the diffusion behavior of the penetrats in any particular system. Furthermore, the quality of the Lorentz-Berthelot mixing rules has not been systematically studied here. We therefore need to address the possibility of inaccuracies in the potentials. We have done this (somewhat arbitrarily) by studying a larger nitrogen molecule in addition to the one described in Table 2. This larger model, hereafter referred to as $N_2L$, was assigned a value of $\sigma$ which is 10% higher than that of the normal nitrogen atom. This has the effect of enhancing the contrast between the penetrants, as discussed later. The choice of 10% is arbitrary, but we believe that it is a reasonable reflection of uncertainty in these potential models.

### *Simulations*

We employed a Monte Carlo method due to Voter (1985) to calculate the free energy differences between oxygen and nitrogen in the pore window, as given by Eq. 9. As applied to our system, Voter's result for the ratio of the two configurational partition functions can be written as

$$\frac{Z_{O_2}}{Z_{N_2}} = \frac{\langle M_\beta \left[ U_{O_2} - U_{N_2} \right] \rangle_{N_2}}{\langle M_\beta \left[ U_{N_2} - U_{O_2} \right] \rangle_{O_2}} \tag{13}$$

$\langle \rangle_{O_2}$ and $\langle \rangle_{N_2}$ represent the canonical ensemble averages with oxygen and nitrogen, respectively, and $M_\beta(\Delta U) \equiv \min[1, \exp(-\beta \Delta U)]$ is the probability of acceptance for a move during which the potential energy changes by $\Delta U$. The

**Table 2. Pure Component LJ Parameters and Center-to-Center Distances**

| Species | $\epsilon$ (kcal·mol$^{-1}$) | $\sigma$ (Å) | $l$ (Å) |
|---|---|---|---|
| N | 0.120 | 3.296 | 1.097 |
| O | 0.150 | 2.940 | 1.169 |
| $CH_3$ | 0.139 | 3.564 | — |

denominator is evaluated by performing a Metropolis Monte Carlo walk (Allen and Tildesley, 1987) with oxygen in the window. During this walk, the center of mass of the oxygen is confined to the plane defining the window; the position of the center of mass within this plane and the rotational degrees of freedom are sampled according to the Metropolis prescription. At regular intervals, ''test moves'' are performed in which the oxygen is turned into a nitrogen, and the probability of acceptance of such a move $M_\beta$ is averaged over the walk. We emphasize that this move is a fictitious one, and does not affect the original Monte Carlo walk of oxygen. The numerator is evaluated in a separate simulation performed in reverse fashion, with a nitrogen walker and test changes to oxygen. In the tighter windows, the average potential energies $\langle U \rangle_{O_2}$ and $\langle U \rangle_{N_2}$ may be quite different from each other, with the latter usually higher than the former. In such instances, the probability of acceptance for the test move of $O_2 \rightarrow N_2$ approaches zero, whereas the reverse move tends to be always accepted. Hence, a shift potential was used to speed convergence of the simulations, as suggested by Voter (1985).

Once the ratio of the configuration integrals is known, the excess free energy difference between oxygen and nitrogen in the window may be simply determined (ref. Eq. 9). By evaluating the excess free energy difference at several temperatures, the individual energetic and entropic contributions may be determined as the intercept and negative slope, respectively, of a line fitted to a plot of excess free energy difference vs. temperature.

Preliminary shorter Monte Carlo runs of approximately $10^5$ moves were carried out for each case to adjust the step sizes and choose the value of the shift potential. Each production Monte Carlo run was typically $5 \times 10^6$ moves long. Simulations were carried out at four different temperatures from 100 to 400 K in steps of 100 K. The resulting plots of excess free energy difference vs. temperature were seen to be linear.

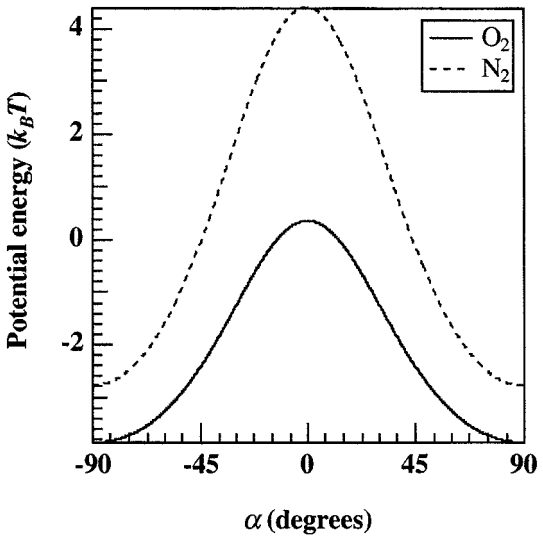


**Figure 2. Potential energy of the penetrants as a function of rotational angle $\alpha$ in a window of size 3.6 Å.**

$T$ is 300 K. Rotation procedure is described in the text.

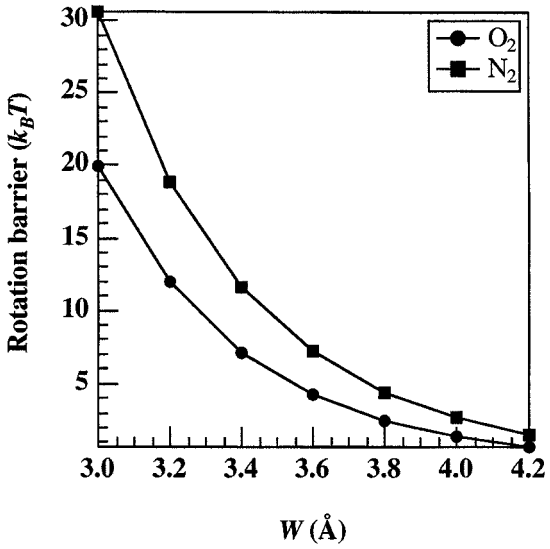


**Figure 3. Rotational barriers ($U_{\alpha=0^\circ} - U_{\alpha=90^\circ}$) as functions of window size.**

$T$ is 300 K.

A least-squares regression analysis was performed on the data to obtain the individual energetic and entropic contributions. All simulations were run with three different starting configurations and the final results were averaged over these sets of independent results. We considered a series of constriction widths ($W$) ranging from 3.0 to 4.2 Å for all models; the energetic selectivities reported are based on $T = 300$ K.

## Results and Discussion

### *Rotational barriers*

Since rotational freedom is an important concept in this problem, the potential energy of each penetrant molecule as a function of orientation is considered first. To study rotational barriers, the molecule is placed parallel to the $x$-axis in the $xy$ plane, with the center of mass fixed at the center of the pore window (that is, location (0,0,0) in Figure 1). Rotation is then performed about the $y$-axis (in the $xz$ plane) with the rotational angle denoted by $\alpha$. Results are shown for a window size $W = 3.6$ Å in Figure 2; plots for other pore sizes are qualitatively similar. An energy maximum occurs at $\alpha = 0°$, where the molecule is in the plane of the window (that is, the $xy$ plane) and overlaps with the solid may be considerable. The molecules have minima in potential energy at $\alpha = \pm 90°$ where the long axis of the molecule is parallel to the $z$ axis (ref. Figure 1), and overlaps with window atoms are minimal in this position. The potential energy values indicate that both penetrants sit comfortably in this window along the axis of the pore.

The value of the rotational barrier, taken as ($U_{\alpha=0^\circ} - U_{\alpha=90^\circ}$), is plotted in Figure 3 as a function of window size. Of course, the barrier for nitrogen is always higher. For pore sizes below approximately 3.8 Å, rotational motion is an activated process for both oxygen and nitrogen, with barrier values exceeding 2.5 $k_BT$ (at $T = 300$ K). The nature of this motion is probably best desribed as vibrational. In the neighborhood of 4.0 to 4.2 Å, there are cases where the rotation of

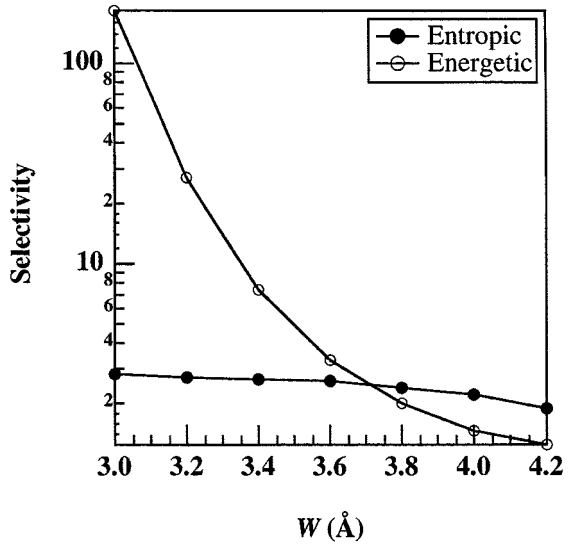


**Figure 4. Energetic selectivity $\exp[-\beta(U_{a,O_2} - U_{a,N_2})]$ and entropic selectivity $\exp[(S_{a,O_2} - S_{a,N_2})/k_B]$ as functions of window size.**

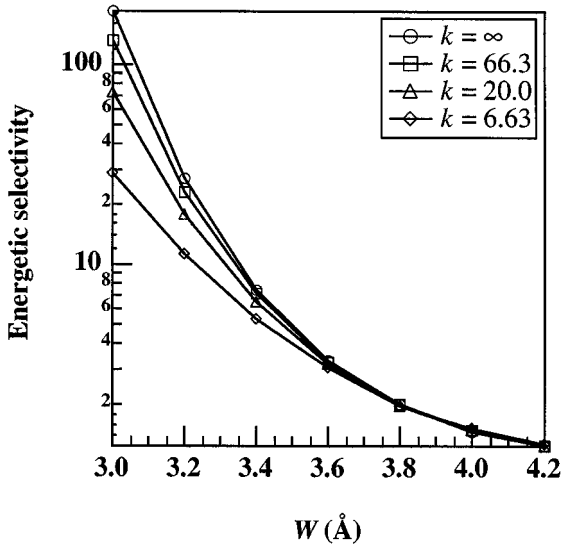


**Figure 5a. Energetic selectivity $\exp[-\beta(U_{a,O_2} - U_{a,N_2})]$ as a function of window size for flexible windows with various spring constants.**

oxygen is free but that of nitrogen is at least hindered, if not activated. For example, at $W = 4.2$ Å, the barrier for oxygen is 0.69 $k_BT$ and that for nitrogen is 1.58 $k_BT$. At $W = 4.0$ Å, the barrier for oxygen is 1.36 $k_BT$ and that for nitrogen is 2.67 $k_BT$. In summary, there is a narrow range of pore sizes for which the rotational motion of oxygen is free but that of nitrogen is more properly characterized as vibrational. However, the activation energies for rotational motion of nitrogen are not particularly high in this regime.

### *Selectivity*

The energetic and entropic components of oxygen/nitrogen selectivity are shown as a function of window width $W$ in Figure 4. As might be expected, both components of selectivity increase as $W$ decreases. However, the energetic component increases rapidly as the window narrows, while the entropic component increases more slowly and even seems to be reaching a plateau. For values of $W$ larger than about 3.7 Å, the entropic selectivity is larger than the energetic selectivity; some experimental results in Table 1b also exhibit such behavior. In contrast to some of the experimental results, entropic selectivity values less than unity are not seen even for very large windows $W > 4$ Å.

The fact that the entropic selectivity is never very high is of great interest. Even in the narrowest window considered here (3 Å), it reaches a value of only 2.8, which is considerably smaller than the value predicted by Singh and Koros with absolute rate theory (14.6). Clearly, the nitrogen molecule is not as ''confined'' relative to the oxygen molecule as they assume. This result is perhaps not surprising in light of the rotational barrier results presented in Figure 3.

### *Effects of window flexibility*

Next we consider the effects of the flexibility of the pore window on the selectivities by employing our flexible solid model. The energetic and entropic selectivities for different values of the bond strength $k$ are presented in Figures 5a and 5b, respectively. The energetic selectivities are lowered as the window flexibility increases, as expected. This effect does not become significant until $W < 3.6$ Å, but it is very large at the smaller window sizes. In contrast, the loss of entropic selectivity with increasing window flexibility is not very significant. Even for $k = 20.0$ kcal mol$^{-1}$ Å$^{-2}$, which represents a very low-frequency motion, entropic selectivities are not very different from the corresponding values in a rigid window. Only for the lowest $k$ does the entropic contribution seem to be significantly affected. The maximum that appears in entropic selectivity near 3.5 Å for this $k$ value is notable.

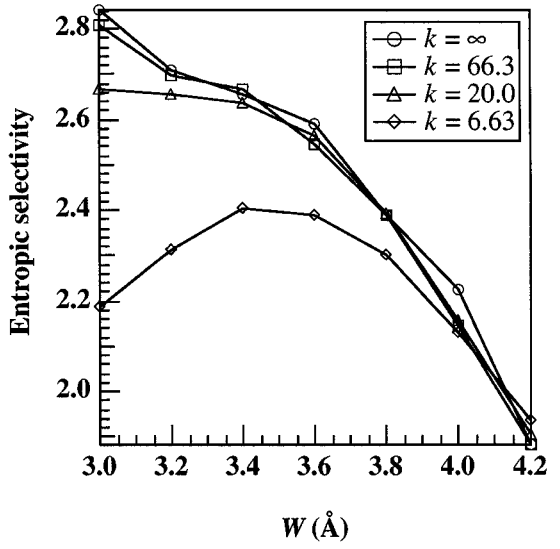


**Figure 5b. As in Figure 5a, but for entropic selectivity $\exp[(S_{a,O_2} - S_{a,N_2})/k_B]$.**

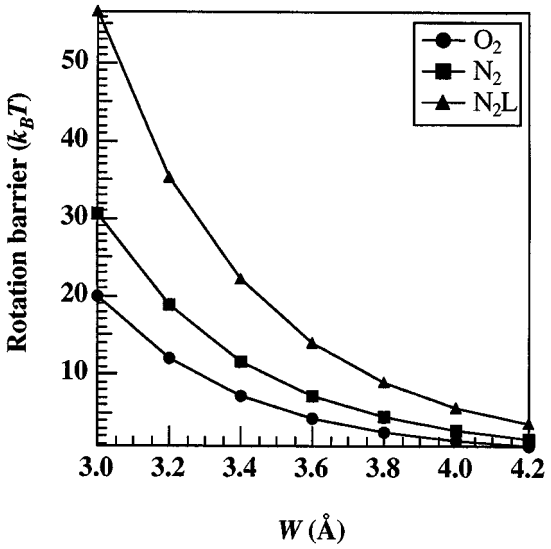


**Figure 6. Rotational barriers ($U_{\alpha=0^\circ} - U_{\alpha=90^\circ}$) as functions of window size.**

$N_2L$ represents a larger version of nitrogen, as described in the text. $T$ is 300 K.

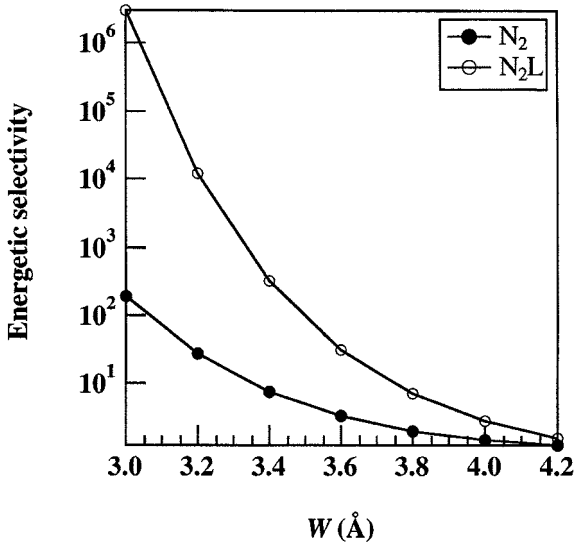


**Figure 7a. Energetic selectivity $\exp[-\beta(U_{a,O_2} - U_{a,N_2})]$ as a function of window size for the AMBER nitrogen model and $N_2L$.**

Here, the solid atoms are so flexible that they can move quite far away from their lattice locations in order to decrease energetic overlaps with the molecule. We believe that this in turn increases the effective width of the window, leading to lower entropic selectivities.

### *Effect of the potential parameters*

As mentioned previously, the potentials used in this study were taken "off the shelf" from the AMBER force-field and other literature sources. Neither the potentials nor the mixing rules were optimized for this diffusion study. Ideally, detailed quantum-mechanical studies could be done on these model systems to evalute the potentials; however, such calculations are very computationally intensive. Another approach is to vary the potential parameters and assess the sensitivity of the results to these changes. The most important variable in the present problem is the difference in the size of the two penetrants, oxygen and nitrogen. Therefore, we studied the separation of oxygen and a "fictitious" nitrogen molecule, referred to as $N_2L$. Each atom in the $N_2L$ molecule was assigned a LJ diameter 10% bigger than that in the original $N_2$, while keeping the $l$ value the same. We believe that a 10% change is sufficient to address uncertainties in the generally accurate AMBER potentials.

First, we shall consider the differences in rotation barriers, as shown in Figure 6; the results from Figure 3 are presented again for comparison. The rotational barriers for $N_2L$ are substantially higher than for AMBER nitrogen; this in turn means that the contrast between the $O_2$ and $N_2L$ is higher compared to that seen earlier for all pore sizes. Another difference is that the $N_2L$ model predicts a larger range of window sizes over which oxygen rotation is nearly free but nitrogen rotation is activated. For example, at a window width of 4.2 Å, the rotation barrier is already 3.5 $k_BT$ for $N_2L$. However, this range is only extended by a few tenths of Angstroms relative to the regular nitrogen model. From this analysis, within the uncertainties of the current potential models, we conclude the following. A pore window in which the rotation of oxygen is free, but the rotational mode of nitrogen becomes vibrational, is possible. However, this will occur only over a very narrow range of pore sizes near 4 Å, and the vibration will be of relatively low frequency.

Due to the increased contrast between the two molecules, one can expect the selectivities calculated for the $O_2/N_2L$ model to be higher compared to those for $O_2/N_2$. The energetic and entropic selectivities for the two models are shown in Figures 7a and 7b, respectively, using the rigid solid. Both selectivities are higher using the $N_2L$ model, as expected, and

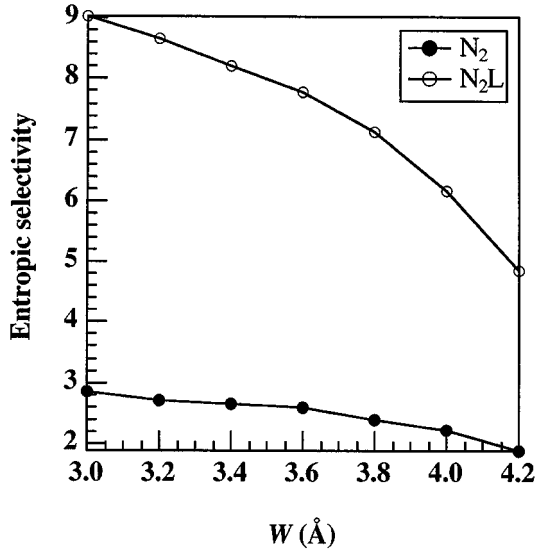


**Figure 7b. As in Figure 8a, but for entropic selectivity $\exp[(S_{a,O_2} - S_{a,N_2})/k_B]$.**

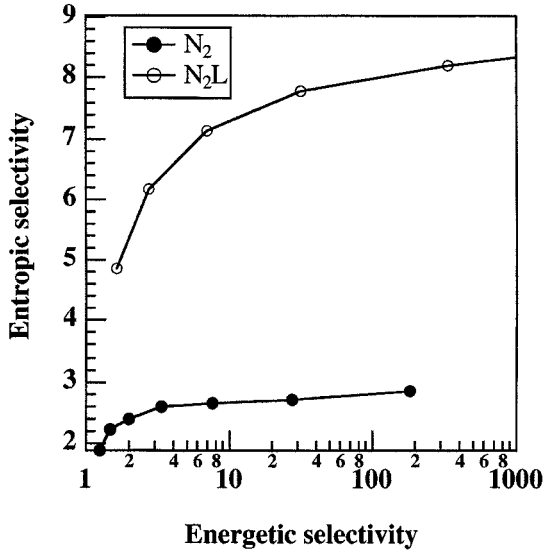


**Figure 8. Entropic selectivity $\exp[(S_{a,O_2} - S_{a,N_2})/k_B]$ as a function of energetic selectivity $\exp[-\beta \times (U_{a,O_2} - U_{a,N_2})]$, for the AMBER nitrogen model and $N_2L$.**

the difference increases as the window size decreases. The difference is quite dramatic in the case of the energetic selectivity with the values differing by nearly 4 orders of magnitude at $W = 3.0$ Å, due to much higher overlaps between the molecule and the solid atoms. Although the difference is not quite as dramatic, the entropic selectivity is also higher with the $N_2L$ model, becoming as large as 9 at $W=3.0$ Å.

An overview of the two models is presented in Figure 8, where entropic selectivity is plotted against energetic selectivity for each, using the rigid solid model. From the experimental data shown in Tables 1a and 1b, we might conclude that a ''plausible'' range of energetic selectivity for the oxygen/nitrogen separation lies between 1 and 30. Based on this information and the results from the AMBER potential in Figure 8, one would expect the entropic selectivity should fall in the range from 2 to 3. Given the uncertainty in the potential models used, as represented by our $N_2L$ calculations, entropic selectivity may actually reach as high as 8. In any case, these values are still significantly smaller than previous estimates (Singh and Koros, 1996) and provide a reasonable guide when interpreting experimental data.

### *Free energy difference in the cages*

As mentioned earlier, we neglected the free energy differences between oxygen and nitrogen in the cages themselves, claiming that this was a reasonable assumption when the cage sizes were large compared to the molecular sizes. Here we derive a rough estimate of the cage effects, in the limit of large cages. For simplicity, we assume that the interaction energy of the penetrant in the cage can be approximated by an average value $\overline{U}$. The configurational integral corresponding to the cage (ref. Eq. A5) can then be rewritten as

$$Z_V = \nu \exp\left(-\beta \overline{U}\right) \tag{14}$$

where $\nu$ is the (hyper)volume swept by the penetrant in all five dimensions. In the limit of large cages, the values of $\nu$ for oxygen and nitrogen will be very close to each other. Hence, the ratio of their volume configurational integrals becomes

$$\frac{Z_{V,N_2}}{Z_{V,O_2}} = \exp\left[-\beta\left(\overline{U}_{N_2} - \overline{U}_{O_2}\right)\right] \tag{15}$$

Next we estimate the potential energy difference in Eq. 15 using the very simple model of a penetrant interacting with a *single* methyl site, identical to the sites that constitute the window. The most favorable (minimum potential energy) position for each penetrant relative to the single methyl site is found, and the potential energy at that position is used as the average energy for that penetrant in Eq. 15. Since an oxygen atom has a slightly larger value of $\epsilon$ than does nitrogen, the potential energy of the oxygen molecule is slightly lower. The actual difference (nitrogen-oxygen) is estimated to be 0.032 kcal/mol, yielding a partition function ratio of 0.95 from Eq. 15 at 300 K. Thus, based on this simple model, we estimate that the effect of the cage contribution would be to lower the overall selectivity by about 5%. Of course, this estimate will change if different assumptions are made regarding the cages. For example, if more cage atoms are considered, the contrast between the interaction energies of the two penetrants will increase to some extent, and the selectivity will be further lowered. More interestingly, as the cages become smaller, the difference between the $\nu$ values for the two penetrants may become significant. Since nitrogen is the larger molecule, its $\nu$ value should generally be lower than that of oxygen, thus resulting in a lowering of the overall entropic selectivity. This last scenario has interesting implications for the entropic selectivities in polymers, since the free volume packets in these materials are typically much smaller than the cages found in the inorganic materials. These effects in polymers will be the subject of future investigation.

### *Present solid model vs. actual zeolite windows*

Some caution must be used when interpreting our results, since they have been based on a particular conceptual model for the structure of a microporous material, namely a three-dimensional isotropic assembly of relatively open cages joined by narrow windows. The effects of size and shape distributions in the cages or windows have not been considered. Furthermore, all of the potential interactions were considered to be of the van der Waals type. Although this model broadly captures the features of many actual materials, significant differences do exist. For example, the windows in 4A zeolites are narrowed by the presence of $Na^+$ ions in the plane of the window. Since oxygen and nitrogen possess finite polarizabilities and quadrupole moments, the presence of ions could significantly modify the nature of the penetrant-window interactions. The effect of such interactions was found to be significant in air separation (Watanabe et al., 1995). The windows considered in the present study are much simpler since the goal here is not to predict the exact separation behavior but rather to investigate the relative importance of energetic and entropic effects in air separation and to directly assess the

influence of structural flexibility on these contributions. For these reasons, *direct* interpretation of the macroscopic behavior of materials which are structurally more complex based on these results may not be appropriate. However, this work should be useful both as a general guide and as a starting point for analysis of different structures.

## Summary

Rigorous expressions for diffusivity-selectivity of oxygen over nitrogen on microporous materials were derived, based on statistical mechanics and transition state theory. These theoretical results were applied to molecular models of oxygen and nitrogen in a simple pore structure, using a Monte Carlo scheme to evaluate the necessary free energy differences. The energetic and entropic contributions to the oxygen/nitrogen separation were resolved and compared to experimental data from the literature. The effects of atomic-level flexibility of the solid were also examined. Furthermore, sensitivity of the results to the parameters in the molecular models was studied.

For a completely rigid solid, entropic selectivities were found to be larger than the energetic contributions for pore windows larger than approximately 3.7 Å; below this pore size, the opposite was true. As window size was decreased, the entropic selectivity appeared to plateau, while the energetic selectivity grew more rapidly. This suggests a point of diminishing returns when attempting to tailor pore size to exploit entropic selectivity. Based on the current best molecular models for oxygen and nitrogen, we predict a maximum entropic selectivity of about 2 to 3. However, accounting for uncertainties in the models, values as high as 8 may be seen. These values are significantly smaller than previous theoretical predictions, but are consistent with experimental data. When atomic-level flexibility was included in the solid model, both energetic and entropic selectivities decreased from the corresponding values in a rigid solid; this effect was much more pronounced for small pore windows. While the energetic selectivity was quite severely affected (especially for small windows), the loss of entropic selectivity was never more than 25%, even for very highly flexible pore structures. These results suggest that intrinsic matrix flexibility may not play as large a role in the entropic aspects of this separation as currently believed. We believe that the geometry of the cages themselves may be important to entropic selectivity, and this will be the subject of future investigation.

## Literature Cited


Allen, M. P., and D. J. Tildesley, *Computer Simulation of Liquids*, Clarendon Press, Oxford (1987).

Auerbach, S. M., and H. I. Metiu, ''Diffusion in Zeolites via Cage-to-Cage Kinetics: Modeling Benzene Diffusion in Na-Y,'' *J. Chem. Phys.*, **105**, 3753 (1996).

Boyd, R. H., and P. V. K. Pant, ''Molecular Packing and Diffusion in Polyisobutylene,'' *Macromol.*, **24**, 6325 (1991).

Chagger, H. K., F. E. Ndaji, M. L. Sykes, and K. M. Thomas, ''Kinetics of Adsorption and Diffusional Characteristics of Carbon Molecular Sieve,'' *Carbon*, **33**, 1405 (1995).

Chihara, K., and M. Suzuki, ''Control of Micropore Diffusivities of Molecular Sieving Carbon by Deposition of Hydrocarbons,'' *Carbon*, **17**, 339 (1979).

Chihara, K., M. Suzuki, and K. Kawazoe, ''Interpretation for the Micropore Diffusivities of Gases in Molecular-Sieving Carbon,'' *J. Colloid Interf. Sci.*, **64**, 584 (1978).

Deem, M. W., J. M. Newsam, and J. A. Creighton, ''Fluctuations in Zeolite Aperture Dimensions Simulated by Crystal Dynamics,'' *J. Amer. Chem. Soc.*, **114**, 7198 (1992).

Farooq, S., ''Sorption and Diffusion of Oxygen and Nitrogen in Molecular Sieve RS-10,'' *Gas Sep. and Purif.*, **9**, 205 (1995).

Gaffney, T. R., ''Porous Solids for Air Separation,'' *Curr. Opin. Solid St. Mat. Sci.*, **1**, 69 (1996).

Glasstone, S., K. J. Laidler, and H. Eyring, *The Theory of Rate Processes*, McGraw-Hill, New York (1941).

Haq, N., and D. M. Ruthven, ''Chromatographic Study of Sorption and Diffusion in 4A Zeolite,'' *J. Colloid Interf. Sci.*, **112**, 154 (1986).

Hill, T. L., *An Introduction to Statistical Thermodynamics*, Dover, New York (1986).

Karger, J., and D. M. Ruthven, *Diffusion in Zeolites and Other Microporous Solids*, Wiley, New York (1992).

McQuarrie, D. A., *Statistical Mechanics*, HarperCollins, New York (1976).

Reid, C. R., I. P. O'koye, and K. M. Thomas, ''Adsorption of Gases on Carbon Molecular Sieves Used for Air Separation. Spherical Adsorptive as Probes for Kinetic Selectivity,'' *Langmuir*, **14**, 2415 (1998).

Robeson, L. M., ''Correlation of Separation Factor versus Permeability for Polymeric Membranes,'' *J. Membrane Sci.*, **62**, 165 (1991).

Ruthven, D. M., ''Adsorption and Diffusion of Nitrogen and Oxygen in a Carbon Molecular Sieve,'' *Chem. Eng. Sci.*, **41**, 1325 (1986).

Ruthven, D. M., and R. I. Derrah, ''Transition State Theory of Zeolitic Diffusion: Diffusion of $CH_4$ and $CF_4$ in 5A Zeolite,'' *J. Chem. Soc. Faraday Trans. I*, **68**, 2332 (1972).

Ruthven, D. M., and R. I. Derrah, ''Diffusion of Monatomic and Diatomic Gases in 4A and 5A Zeolites,'' *J. Chem. Soc. Faraday Trans. I*, **71**, 2031 (1975).

Singh, A., and W. J. Koros, ''Significance of Entropic Selectivity for Advanced Gas Separation Membranes,'' *Ind. Eng. Chem. Res.*, **35**, 1231 (1996).

Snurr, R. Q., A. T. Bell, and D. N. Theodorou, ''A Hierarchical Atomistic/Lattice Simulation Approach for the Prediction of Adsorption Thermodynamics of Benzene in Silicalite,'' *J. Phys. Chem.*, **98**, 5111 (1994).

Stern, S. A., ''Polymers for Gas Separations: The Next Decade,'' *J. Memb. Sci.*, **94**, 1 (1994).

Theodorou, D. N., and U. W. Suter, ''Atomistic Modeling of Mechanical Properties of Polymeric Glasses,'' *Macromolecules*, **19**, 139 (1986).

Voter, A. F., ''Monte Carlo Method for Determining Free-Energy Differences and Transition State Theory Rate Constants,'' *J. Chem. Phys.*, **82**, 1890 (1985).

Watanabe, K., N. Austin, and M. R. Stapleton, ''Investigation of the Air Separation Properties of Zeolites Type-A, Type-X and Type-Y by Monte-Carlo Simulations,'' *Mol. Sim.*, **15**, 197 (1995).

Weiner, S. J., P. A. Kollman, D. T. Nguyen, and D. A. Case, ''An All Atom Force-Field for Simulations of Proteins and Nucleic-Acids,'' *J. Comput. Chem.*, **7**, 230 (1986).


## Appendix A: Window and Volume Partition Functions for Rigid Diatomic Molecules

A rigid diatomic molecule has five degrees of freedom in the normal state: translation in $x$, $y$ and $z$ directions and rotation around the two axes of symmetry. Following McQuarrie (1976), the classical partition function of such a molecule in an adsorption site can be written as

$$Q_V = \frac{1}{h^5}\int_{-L/2}^{L/2} dx \int_{-L/2}^{L/2} dy \int_{-L/2}^{L/2} dz \int_0^{\pi} d\theta \int_0^{2\pi} d\phi \int_{-\infty}^{\infty} dp_x \int_{-\infty}^{\infty} dp_y$$

$$\times \int_{-\infty}^{\infty} dp_z \int_{-\infty}^{\infty} dp_\theta \int_{-\infty}^{\infty} dp_\phi \, e^{-\beta H(x,y,z,\theta,\phi,p_x,p_y,p_z,p_\theta,p_\phi)} \quad \text{(A1)}$$

where $\theta$ and $\phi$ are the Eulerian angles, the $p_i$ are the momenta of the molecule in the respective degrees of freedom, and $H$ is the classical Hamiltonian

$$H = \frac{1}{2m}\left(p_x^2 + p_y^2 + p_z^2\right) + \frac{1}{2I}\left(p_\theta^2 + \frac{p_\phi^2}{\sin^2\theta}\right) + U(x,y,z,\theta,\phi) \tag{A2}$$

where $m$ and $I$ are the mass and moment of inertia of the molecule, respectively. $U$ is the potential energy of the molecule due to its interactions with the solid, which will generally be a function of position and orientation. Since potential and kinetic energies are decoupled in the classical limit, we have

$$Q_V = q_V Z_V \tag{A3}$$

where $q_V$ is given by

$$q_V = \left(\frac{2\pi m k_B T}{h^2}\right)^{3/2}\left(\frac{2\pi I k_B T}{h^2}\right) \tag{A4}$$

and $Z_V$ is the classical configuration integral

$$Z_V = \int_{-L/2}^{L/2} dx \int_{-L/2}^{L/2} dy \int_{-L/2}^{L/2} dz \int_0^{\pi} \sin\theta\, d\theta \int_0^{2\pi} d\phi\, e^{-\beta U(x,y,z,\theta,\phi)} \tag{A5}$$

The first quantity in Eq. A4 comes from the translational momenta and the second from rotational momenta. All of the influence of the solid on the adsorbed molecule is captured in Eq. A5.

We now consider the partition function for a gas molecule whose center of mass is confined to a ''window'' as it moves from one cage to the next. For convenience, we consider the window to lie in the $xy$ plane; thus, the $z$ contributions to the partition function disappear, and we have

$$Q_A = \frac{1}{h^4}\int_{-W/2}^{W/2} dx \int_{-W/2}^{W/2} dy \int_0^{\pi} d\theta \int_0^{2\pi} d\phi \int_{-\infty}^{\infty} dp_x \int_{-\infty}^{\infty} dp_y \times \int_{-\infty}^{\infty} dp_\theta \int_{-\infty}^{\infty} dp_\phi\, e^{-\beta H(x,y,\theta,\phi,p_x,p_y,p_\theta,p_\phi)} \tag{A6}$$

As in the case of the partition function in the adsorption site, the partition function in the window can be written in a simplified form as

$$Q_A = q_A Z_A \tag{A7}$$

where

$$q_A = \left(\frac{2\pi m k_B T}{h^2}\right)^{2/2}\left(\frac{2\pi I k_B T}{h^2}\right) \tag{A8}$$

and

$$Z_A = \int_{-W/2}^{W/2} dx \int_{-W/2}^{W/2} dy \int_0^{\pi} \sin\theta\, d\theta \int_0^{2\pi} d\phi\, e^{-\beta U(x,y,\theta,\phi)} \tag{A9}$$

Note that the exponent in Eq. A8 is 2/2, in contrast to the 3/2 seen in Eq. A4, reflecting the reduction in the number of degrees of freedom in the window.

## Appendix B: Form of the Model Potential

The modified LJ potential used in this work is described by the following set of equations

$$U_{ij}^{LJ} = 4\epsilon_{ij}\left[\left(\frac{\sigma_{ij}}{r_{ij}}\right)^{12} - \left(\frac{\sigma_{ij}}{r_{ij}}\right)^{6}\right] \qquad r_{ij} < R_1 \tag{B1}$$

$$= \epsilon\left(1-\xi^3\right)\left\{A_0 + A_1\xi + A_2\xi^2\right\} \qquad R_1 < r_{ij} < R \tag{B2}$$

where

$$A_0 = \left.\frac{U_{ij}^{LJ}}{\epsilon}\right|_{r_{ij}=R_1} \tag{B3}$$

$$A_1 = \left.\left(3\frac{U_{ij}^{LJ}}{\epsilon} + \Delta\frac{\left(U_{ij}^{LJ}\right)'}{\epsilon/\sigma}\right)\right|_{r_{ij}=R_1} \tag{B4}$$

$$A_2 = \left.\left(6\frac{U_{ij}^{LJ}}{\epsilon} + 3\Delta\frac{\left(U_{ij}^{LJ}\right)'}{\epsilon/\sigma} + \frac{\Delta^2}{2}\frac{\left(U_{ij}^{LJ}\right)''}{\epsilon/\sigma^2}\right)\right|_{r_{ij}=R_1} \tag{B5}$$

$$\xi = \frac{\left(r_{ij} - R_1\right)}{R} \tag{B6}$$

and

$$\Delta = \frac{\left(R - R_1\right)}{\sigma} \tag{B7}$$

The primes in the above equations denote derivatives with respect to the center-to-center distance $r_{ij}$. $R_1 = 1.5\sigma$ and $R = 3.5\sigma$ are used in this study.

*Manuscript received June 3, 1999, and revision received Sept. 13, 1999.*